RSC Advances

PAPER

View Article Online
View Journal | View Issue

Cite this: *RSC Adv.*, 2018, **8**, 19449

A comparative study on the electrochemical properties of nanoporous nickel oxide nanowires and nanosheets prepared by a hydrothermal method†

Kien Nguyen, Nguyen Duc Hoa,* Chu Manh Hung, Dang Thi Thanh Le, Nguyen Van Duy and Nguyen Van Hieu

Metal oxide nanostructures have been extensively used in electrochemical devices due to their advantages, including high active surface area and chemical stability. However, the electrochemical properties of metal oxides are strongly dependent on their structural characteristics. We performed a comparative study on the electrochemical performance of nanoporous nickel oxide (NiO) nanosheets and nanowires. The advanced nanoporous NiO nanomaterials were synthesized by a facile hydrothermal method followed by thermal calcination. The synthesized nanomaterials, as characterized by scanning electron microscopy, transmission electron microscopy, selected area electron diffraction, X-ray diffraction, and nitrogen adsorption/desorption isotherms, demonstrated the nanoporosity and high crystallinity of the NiO nanosheets and nanowires. Cyclic voltammetry measurement was performed using a three-electrode system to evaluate the electrochemical properties of the synthesized materials. Results showed that the nanoporous NiO nanosheets possessed a higher current density than that of the nanowires by approximately ten times. Moreover, the nanoporous NiO nanosheets showed exceptionally high stability of almost 100%, after three cycles in strong alkaline environments, thereby suggesting possible application in electrochemical devices.

Received 3rd April 2018
Accepted 20th May 2018

DOI: 10.1039/c8ra02862a

rsc.li/rsc-advances

1. Introduction

Environmental pollution and lack of energy are the most concerning issues in modern society due to the intermittent usage of fossil fuels.[1] Thus, replacing fossil fuels and reducing environmental pollution by exploiting new green energy sources is a crucial and effective pathway.[2] Extensive studies have attempted to achieve efficient technologies for energy storage and conversion by using advanced nanomaterials.[3] Some common devices for this purpose are rechargeable batteries and supercapacitors, and the latter are becoming high-potential energy storage devices due to their high energy density, long life cycle, and fast recharge cycle.[4] To maximize the capacitance, increasing the effective surface area of the electrode materials is one of the key solutions. Thus, scientists have tried improving capacitive performance by exploring effective electrode materials with novel morphologies that can maximize cycling stability, charge/discharge rate capability, and safety of usage.[5,6] Different materials were used for supercapacitor electrodes such as $Ni(OH)_2$ hollow spheres,[7] three-dimensional bubble-like graphene frameworks,[8] porous graphene frameworks,[9] and composites of MoS_2, reduced graphene oxide and NiO.[10] Nanostructured materials that have been studied for this purpose include carbon-based materials[11] and conducting polymers.[12] However, these materials have disadvantages, such as high resistivity (carbon-based materials) and easy mechanical degradation (conducting polymers), both of which may lead to decreased capacitance.[13] In contrast, metal oxides, such as NiO, MnO_2, $FeCo_2O_4$, Co_3O_4, and CuO, have been considered as options due to their high energy density, excellent electrochemical performance, and thermal and chemical stability.[14–16]

Nickel oxide (NiO) is one of the most promising choices owing to its environmental friendliness, low cost, easy preparation, high theoretical specific capacitance (3750 F g^{-1}),[17] and excellent electrochemical reversibility.[18,19] Scientists have tried preparing NiO with different morphologies, such as nanoparticles,[20] nanowires,[21] nanosheets,[22] and nanorods,[23] which can improve electrochemical performance. Regarding fabrication techniques, finding a simple and practicable method for the large-scale synthesis of NiO nanostructures that can control morphology and quality of materials is highly important. Compared with other methods, such as sol–gel,[24] electrodeposition,[25] template synthesis,[26] and chemical precipitation,[27] the

International Training Institute for Materials Science (ITIMS), Hanoi University of Science and Technology (HUST), No 1 – Dai Co Viet Str. Hanoi, Vietnam. E-mail: ndhoa@itims.edu.vn

† Electronic supplementary information (ESI) available. See DOI: 10.1039/c8ra02862a

hydrothermal method[28] is of particular interest and thus has been explored widely for synthesizing NiO nanostructures. This method can be carried out in simple conditions without the need of high vacuum condition.[29] Jiang *et al.*[30] reported on the fabrication of NiO nanorods on nickel foam by hydrothermal method, in which the foam can be used as both substrate and Ni source. Moreover, scientists can easily alter the size and morphology of materials with the hydrothermal method by varying the synthesis condition. Cao *et al.*[31] studied the effects of sodium oxalate in the synthesis for NiO nanobelts, and pointed out that the diameter of nanobelts could be increased to from 80 to 100 nm just by adjusting the amount of sodium oxalate. Safa *et al.*[32] synthesized NiO with different morphologies by varying the synthesis temperature from 100 °C to 220 °C to obtain nanoparticles, nanorods, and nanoworms. Li.*et al.*[33] reported on the synthesis of $Ni(OH)_2$ nanowalls and decomposed the synthesized materials into NiO. The NiO nanoparticles of different sizes and porosities were synthesized by using the hydrothermal method, and their electrochemical performances were inversely dependent on the band gaps. It was obviously that the electrochemical properties of the nanostructured NiO were clearly strongly dependent on the material morphologies. However, none of these reports were dedicated to the synthesis and systematic comparison of the electrochemical properties of NiO nanowires and nanosheets.

In this study, nanoporous NiO nanosheets and nanowires were prepared by using the hydrothermal method for supercapacitor applications. The facile hydrothermal synthesis and subsequently calcination enables the porous structure NiO with high crystallinity. The electrochemical properties of the synthesized materials were investigated by using cyclic voltammetry (CV) techniques for comparison. Moreover, we addressed the relationship among the morphology, specific surface area, and electrochemical properties of the synthesized NiO nanomaterials.

2. Experimental process

2.1 Synthesis of NiO nanowires

The NiO nanowires were synthesized using the hydrothermal method at 200 °C.[34] In a typical synthesis, 0.47 g $NiCl_2 \cdot 6H_2O$ was dissolved into a mixture of 32 mL ethylene glycol and 18 mL deionized (DI) water in a beaker under continuous magnetic stirring at room temperature. Afterward, 0.12 g $Na_2C_2O_4$ was added into the beaker and the mixture was stirred for 1 hour to disperse the Ni^{2+} ions homogeneously before being poured into the 100 mL autoclave and heating at 200 °C for 24 hours. After the heating treatment, the autoclave was naturally cooled to room temperature and the products were collected by centrifugation; afterward, the products were washed 5 times with DI water and ethanol. The light-blue-green product was collected and dried in air at 50 °C for about 24 h. The polycrystalline NiO nanowires were obtained by calcinating this product ($NiC_2O_4 \cdot 2H_2O$) at 400 °C for 2 hour in air.

2.2 Synthesis of NiO nanosheets

The NiO nanosheets were synthesized by hydrothermal method without using surfactants or structure-directing agents.[35] In this process, 1.29 g anhydrous nickel chloride was dissolved in DI water to obtain a light-green solution. Afterward, the ammonia solution was added under magnetic stirring to adjust the pH of the solution to the value of 10. Subsequently, the solution was poured into a 100 mL autoclave for hydrothermal treatment. The hydrothermal process was done at 160 °C for 6 hours and then cooled to room temperature naturally. Later, the precipitate was collected and washed 5 times with DI water and ethanol to remove the unreacted agents and impurities, and the products were collected by centrifugation at 4000 rpm. The precipitate was dried at 45 °C overnight and finally calcined at 400 °C for 2 hour in air to obtain NiO nanosheets.

2.3 Electrochemical measurement

A three-electrode cell system was used to evaluate the electrochemical performance of the prepared materials through CV measurement using a potentiostat/galvanostat instrument (Ivium Vertex). The CV was measured at room temperature using Pt wire and Ag/AgCl as counter and reference electrodes, respectively. The working electrode was prepared by mixing NiO nanowires or nanosheets with polytetrafluoroethylene (PTFE) at a weight proportion of 10 : 1 before being pressed into a thin sheet of uniform thickness. The thin sheets were then loaded on a nickel foam to act as a current collector for CV measurement. Potassium hydroxide solution (1 M) was used as the electrolyte, whereas the CV curves were measured at different scan rates from 10–50 mV s^{-1}.

2.4 Material characterization

The synthesized materials were characterized by using advanced techniques, such as scanning electron microscopy (SEM), transmission electron microscopy (TEM), selected area electron diffraction (SAED), and X-ray diffraction (XRD). The specific surface areas of the two samples were measured using Brunauer–Emmet–Teller (BET) method (Micrometrics Gemini VII).

3. Result and discussion

3.1 Material characteristics

Previous reports have shown that altering the material structure can lead to changes in the electrochemical performance of the samples.[22,28] Thus, in this study, NiO nanosheets and nanowires were prepared by hydrothermal method under different conditions. Morphology of the hydrothermal nanowires before calcination characterized by SEM and TEM images are shown in Fig. S1 (ESI†). The nanowires are very homogenous with diameter of about 40 nm. The TEM images reveal that the nanowires are composed of nanocrystals of about 10 nm in size. The gap between lattice fringes is 0.24 nm, corresponding to the interspace of (111) planes of monoclinic nickel oxalate hydrate (Fig. S2, ESI†). SEM and TEM images of the hydrothermal nanosheets before calcination are shown in Fig. S3 (ESI†). The nanosheets have a hexagonal shape with an average diameter of about 250 nm, and thickness of 25 nm. The hydrothermal nanosheets are highly crystallinity, in which the interspace between two lattice fringes is 0.238 nm, corresponding to the

interspace of (101) planes of nickel(II) hydroxide (Fig. S4, ESI†). Morphologies of the NiO nanosheets and nanowires obtained after calcination characterized by SEM images are shown in Fig. 1. The NiO nanosheets (Fig. 1(A)) have a hexagonal shape with an average size of approximately 250 nm in diameter and about 25 nm in thickness. The materials were highly homogenous and no other structures were observed in the sample. In addition, the NiO nanosheets showed porous structures, and air voids formed in the material surface (Fig. 1(A)). The formation of porous structures was ascribed to the weight loss during calcination.[36] The SEM image of the as-synthesized NiO nanowires in Fig. 1(C) shows that the products conglomerated into nanowires with a high-density porous structure. Moreover, the diameter of NiO nanowires are approximately 50 nm, with an average length of approximately 2 μm. Furthermore, the nanowires showed high porosity due to the formation of tiny nanograins (Fig. 1(D)). Each grain was approximately 10 nm in diameter. The porous structure of a material is highly important in enhancing its electrochemical properties because the porosity provides increased the effective specific surface area. The SEM images revealed that nanowires have a higher porosity than nanosheets.

The as-prepared NiO products were further characterized by TEM, as shown in Fig. 2. The TEM images of NiO nanosheets revealed a dish-like morphology with hexagonal shapes, which was consistent with the SEM observation (Fig. 2(A)). The angle of the hexagonal nanosheet was approximately 120°. However, some nanosheets have a curvature shape, in which the edge angle is larger than 120°. The porous nature of the nanosheets can be seen in the TEM image. The inset of Fig. 2(A) is the corresponding selected area of electron diffraction that confirms the high crystallinity of the nanosheet. The HRTEM image of the nanosheet in Fig. 2(B) reveals the clear lattice fringes of cubic NiO crystals with different orientation. Moreover, the gaps between lattice fringes were approximately 0.15 and 0.24 nm, which correspond to the interspace of (220) and (111) planes, respectively.[37] The TEM image of NiO nanowires in Fig. 2(C) demonstrate that the nanowires have an average

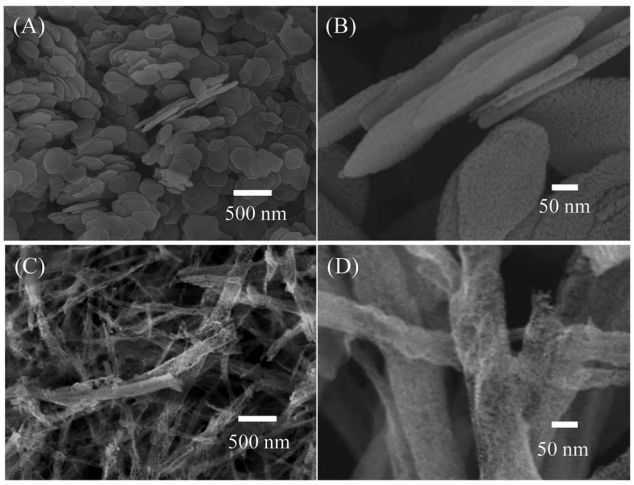

Fig. 1 SEM images of synthesized NiO (A and B) nanosheets, and (C and D) nanowires.

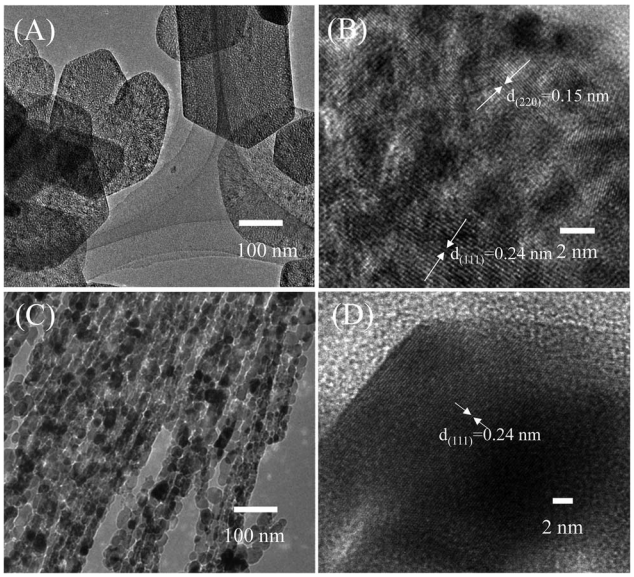

Fig. 2 TEM images of synthesized porous NiO (A and B) nanosheets, and (C and D) nanowires. Insets are corespondent selected area electron diffraction.

diameter of approximately 20 nm with the length up to micrometers. Additionally, the nanowire was assembled from nanograins of about 20 nm in diameter. The HRTEM image of the nanowire is shown in Fig. 2(D). It is different from the nanosheet, the lattice fringes of the nanowire were uniformly distributed on the surface of NiO crystal. The interplanar spacing value was 0.24 nm and belongs to the interspace of (111) planes of cubic NiO. This result suggested that the preferred exposure facet of the NiO nanowire was {111} but not the {220} as that in the nanosheets.[36] The difference in exposure facets can influence the electrochemical properties of a material, as pointed out in ref. 38.

Fig. 3 illustrates the typical powder XRD patterns of the as-prepared NiO nanosheets and nanowires. The differences are slight in the XRD patterns of the two samples because their chemical compositions and physical and chemical properties are similar.[22] Moreover, both samples show typical diffraction peaks at $2\theta = 37.3$, 43.4, and 62.9°, which were indexed to the (111), (200), and (220) of the face-centered cubic unit cell, respectively, with a lattice parameter of 0.417 nm (JCPDS card No. 47-1049). The intensity of (200) peak was the highest, followed by those of (111) and (220) peaks. The average crystalline sizes estimated from XRD data using Scherrer equation were 16.97, and 18.80 nm for nanosheets and nanowires, respectively.[39] Combined with HRTEM results, it can suggest that the NiO nanosheet was composed of nanocrystals (~16.97 nm) of different orientations, whereas the nanowire was composed of different single crystals.

The specific surface area and porosity of hydrothermal products, NiO nanosheets and nanowires were investigated by using nitrogen adsorption/desorption isotherms. The hydrothermal nanowires and nanosheets have nonporous structure as illustrated in Fig. S5 and 6, respectively (ESI†). The BET surface areas of the hydrothermal nanowires and nanosheets

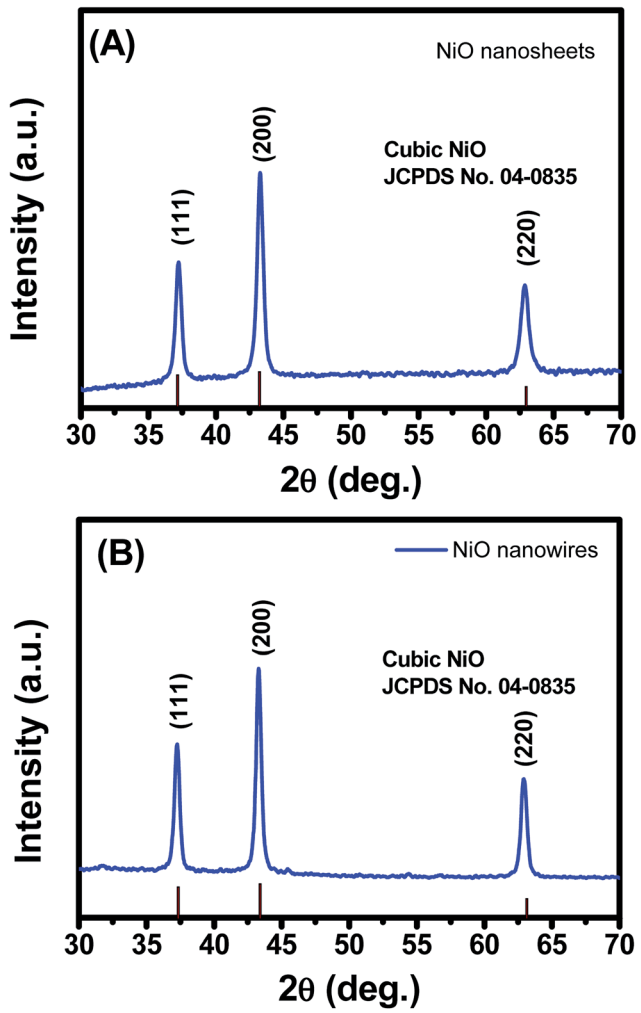

Fig. 3 XRD patterns of synthesized porous NiO (A) nanosheets and (B) nanowires.

are about 6.2, and 4.1 $m^2\ g^{-1}$, respectively. The isotherm nitrogen adsorption/desorption of NiO nanosheets (Fig. 4(A)) showed low hysteresis with a small H1-type loop, thus reflecting the mesoporous nature of the NiO nanosheets. Enlargement of Fig. 4(A) confirms the hysteresis loop of the nitrogen adsorption/desorption isotherm of NiO nanosheets (Fig. S8, ESI†). This result is consistent with other report on the hexagonal mesoporous NiO nanoplates.[38] The pore size distribution curve is shown in the inset of Fig. 4(A), which exhibits a single peak centered at 7.2 nm, thus demonstrating the uniformity of pore size. The specific BET surface area and total pore volume were 61.6 $m^2\ g^{-1}$ and 0.225 $cm^3\ g^{-1}$, respectively. The isotherm nitrogen adsorption/desorption of NiO nanowires (Fig. 4(B)) was similar to that of the nanosheets but without the hysteresis loop, suggesting the non-microporous behavior of the nanowires.[40] The specific BET surface area and total pore volume were determined to be approximately 31.18 $m^2\ g^{-1}$ and 0.169 $cm^3\ g^{-1}$, respectively. The pore size distribution of the nanowire sample showed a small peak centered at about 10.5 nm, as a result of the air gap between the inter grains.[40] This result was consistent with the TEM characterization because the nanowire was formed by the different nanograins.

3.2 Electrochemical properties

The electrochemical properties of the NiO nanosheets and nanowires were characterized by using their CV profiles for comparison. Fig. 5 illustrates the comparison results of the electrochemical performance of NiO nanowires and nanosheets at different scan rates from 10–50 mV s^{-1}. As seen in Fig. 5, the CV curves of both samples possess two redox peaks, namely, the anodic and cathodic peaks at the potential values approximately −0.55, and −0.88 V, respectively. The anodic peak results from the electron transfer reaction, as follows:

$$Ni^{2+} \rightarrow Ni^{3+} + e^- \quad (1)$$

While the cathodic peak results from the following reaction:

$$Ni^{3+} + e^- \rightarrow Ni^{2+} \quad (2)$$

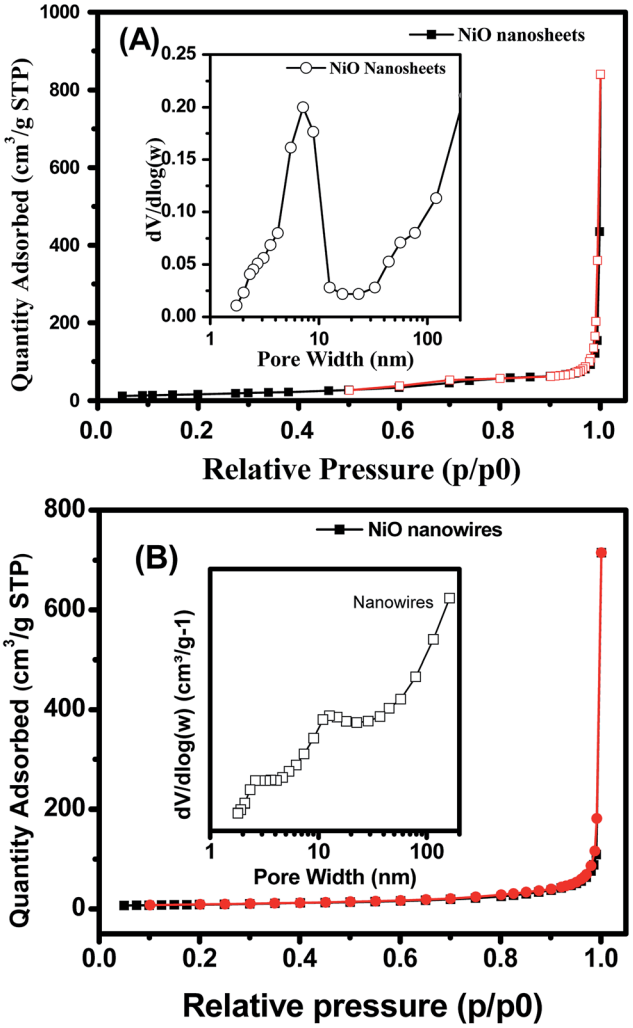

Fig. 4 Nitrogen adsorption/desorption of NiO (A) nanosheets, and (B) nanowires. Insets are pore size distributions.

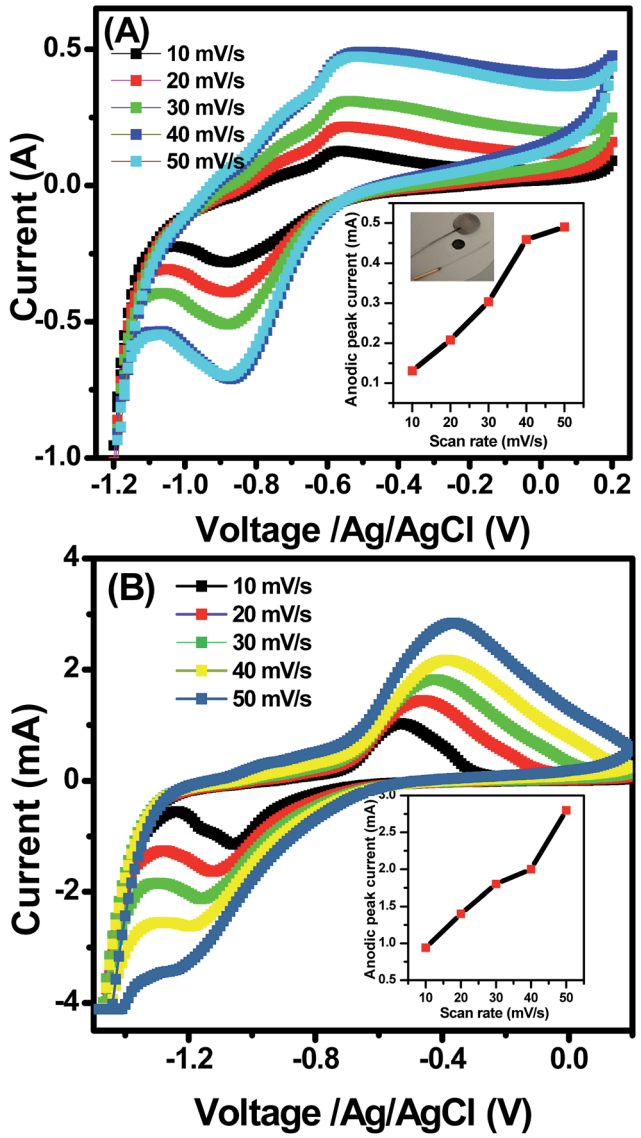

Fig. 5 Cyclic voltammetry of synthesized porous NiO (A) nanowires, and (B) nanosheets at different scan rates (10–50 mV s^{-1}). Insets are plots of anodic peak current *versus* scan rate.

The CV curves show unsymmetrical redox peaks that indicate the quasi-reversible redox process of the NiO products. There was negligible shifts in anodic and cathodic peak potentials at different scan rates in the nanowires (Fig. 5(A)). However, the results are different in the nanosheets (Fig. 5(B)). With increase of scan rate from 10–50 mV s^{-1}, the absolute potential value of anodic peak decreases whereas that value of cathodic peak increases. Those results indicate that the electron transfer process of the redox reactions was dependent on the voltage scan rate, causing by the polarization in the electrode material.[17,41] Ibrahim *et al.*[42] measured the CV curve of NiO nanowires within the potential window of −1 to 1 V at the scan rate of 50 mV s^{-1}, and their result showed that the small peak was obtained at approximately 0.5 V. Vidhyadharan *et al.*[43] prepared NiO nanowires *via* the electrospinning method for supercapacitor application, where they measured the CV curves within the potential window from 0–0.5 V at different scan rates and observed the unsymmetrical redox peaks from 0.175 to 0.45 V. The electrochemical properties of the NiO nanosheet were also studied extensively. Xiao *et al.*[22] prepared NiO nanosheet assemblies for supercapacitors, wherein they measured the CV curves within a potential range of −0.2 to 0.25 V at different scan rates; they found weak redox peaks as a result of the faradic pseudocapacitance behavior. Lee *et al.*[44] synthesized NiO nanosheets based microspherical structures by using the template-free method for supercapacitors, where they observed the cathodic and anodic peaks at potentials of 0.21 and 0.31 V, respectively. In our study, the cathodic and anodic peaks occurred at potentials of approximately −0.88 and −0.5 V, respectively. Insets of Fig. 5(A) and (B) show the plots of anodic peak currents *versus* the scan rates of two samples, respectively. When the scan rate increase from 10 to 50 mV s^{-1}, the anodic peak currents of nanowires increased from 0.13 to 0.49 mA, whereas those of the nanosheets increased from 0.93 to 2.8 mA. In the electrochemically reversible electron transfer processes, the peak current i_p (A) is described by the Randles–Sevcik equation.[45]

$$i_p = 0.446nFAC_0\left(\frac{nFvD_0}{RT}\right)^{1/2} \quad (3)$$

where v (Vs^{-1}) is the scan rate, n is the number of electrons transferred in the redox event, A (cm^2) is the electrode surface area, D_0 (cm^2 s^{-1}) is the diffusion coefficient of the oxidized analyte, and C_0 (mol cm^{-3}) is the bulk concentration of the analyte. Comparing the *C*–*V* data of the NiO nanosheets and nanowires (Fig. 5(A) and (B)), we can assume that the difference in peak current of two samples is mainly caused by the differences in the number of electron transferred. The peak current of nanosheets is higher than that of the nanowires, suggesting that the electron transferred in NiO nanosheets is easier than that in the nanowires. The anodic peak current of nanosheets was higher than that of the nanowires, suggesting the potential application of nanosheets for electrochemical water treatment or chemical sensors.[46] In addition, the specific capacitance C (Fg^{-1}) is one of the most important parameters for evaluating the electrochemical performance of supercapacitors, which can be calculated using the following formula:[7]

$$C = \frac{1}{mv(V_c - V_a)}\int_{V_a}^{V_c} I(V)\mathrm{d}V \quad (4)$$

where m (g) is the mass of the electroactive material in the electrodes, v (mV s^{-1}) is the potential scan rate, V_a (V) is the starting potential, V_c (V) is the ending potential, and I (V) is the response current density (A). The specific capacitances of NiO nanosheets and nanowires at scan rates of 10 mV s^{-1} calculated to be about 87.25 × 10^{-5} Fg^{-1} and 23.66 × 10^{-5} Fg^{-1}, respectively. Such those values are lower than the theoretical specific capacitance of NiO (3750 F g^{-1}).[17] But anyhow, the results confirm that the specific capacitances of NiO nanosheets is 3.68 times higher than that of the nanowires, thus suitable for application in supercapacitor or electrochemical devices.

From the observed CV curves, we studied the electrochemical performance of the nanosheet samples with respect to

the electrochemical performance of the nanowire by comparing them at a specific scan rate, which in this case was 10 mV s^{-1}, and the result is shown in Fig. 6(A). Regarding the anodic peak, the value of NiO nanosheets was 0.94 mA, whereas that of nanowires was only 0.124 mA. For the cathodic peak, the peak appeared at approximately −0.5 mA for the nanowires, whereas that of the nanosheet was approximately −1.3 mA. From these two results, the current of the NiO nanosheet sample was remarkably higher than that of NiO nanowires, thereby indicating a substantial domination of NiO nanosheet electrochemical capacitance; this phenomenon can be explained to be a result of the enhanced surface area of the nanosheet compared with the nanowire structure, as indicated above, which increased the active area for the redox reaction to happen.[47] The nanosheet sample had the higher electrochemical performance; therefore, we continued to investigate its stability by recording the CV curves 3 times at 50 mV s^{-1}, as in the Fig. 6(B). In Fig. 6(B), the 3 lines match each other perfectly, indicating the high stability of the sample. However, with increase of cycling test, the redox peaks disappeared, and the materials were detached from the electrode due to the weak adhesion between the materials and the electrode (Fig. S8, ESI†). It is believed that for practical application as electrodes in a supercapacitor, the cycling test should be stabled up to 10 000 cycles.[8] Thus increase the stability of the device is necessary, and this work is under studying and the data will be reported elsewhere. The electrochemical impedance spectroscopy of NiO nanosheets and nanowires was also studied, and the Nyquist plots are shown in Fig. S9 (ESI†). It is clearly that the Nyquist plots both samples look like two semicircles of different radiuses. This is the result of the parallel arrangement of resistor and capacitor in the device. Different radiuses are caused by different values of resistor and capacitor of the electrodes.

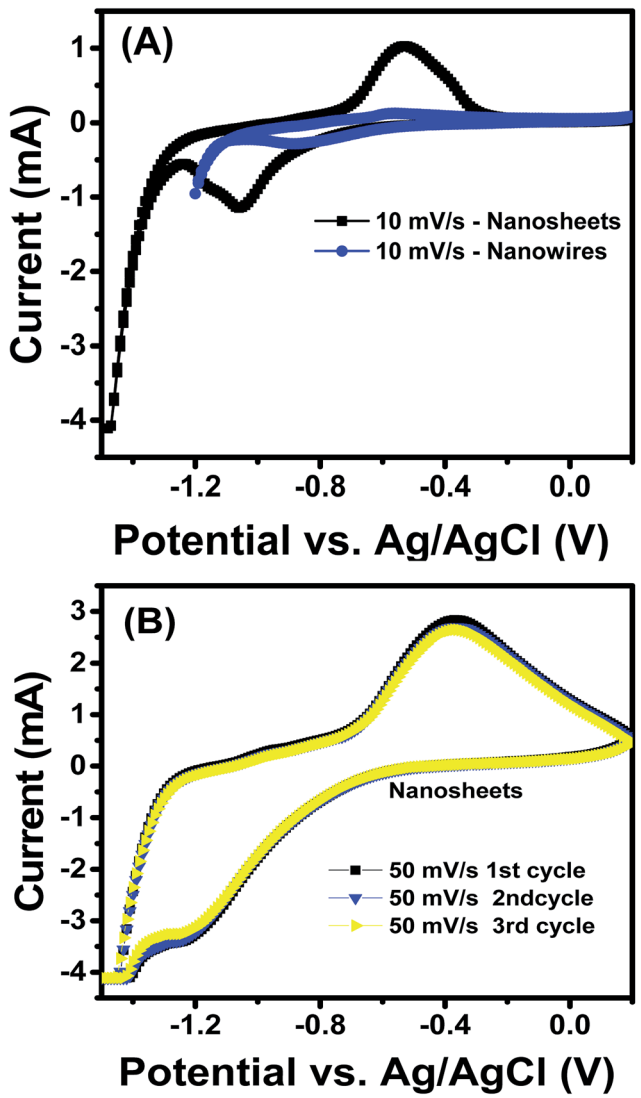

Fig. 6 (A) a comparative cyclic voltammetry of porous NiO nanowires and nanosheets at the scan rate of 10 mV s^{-1}; (B) cyclic voltammetry of NiO nanosheets at scan rate of 50 mV s^{-1} after 3 cycles.

4. Conclusion

In this study, we successfully fabricated nanoporous NiO nanowires and nanosheets by using hydrothermal method and subsequent calcination. Materials were characterized by advanced techniques, such as XRD, SEM, TEM, and BET, as well as CV and EIS measurements. The results pointed out that the morphology of materials significantly influence their electrochemical properties, in that the NiO nanosheets showed superior performance in terms of current density and resulted in redox peaks. Moreover, the nanosheets exhibited significantly high stability after 3 cycles with a conservation value of nearly 100%. Furthermore, this study concluded that the nanoporous NiO nanosheets are advantage for electrochemical applications and can be applied for energy storage devices, especially as electrode materials for supercapacitors or batteries.

Conflicts of interest

There are no conflicts to declare.

Acknowledgements

This work was financially supported by the Ministry of Science and Technology, under the Grant No. ĐTĐLCN.21/17. Authors thank associate professor Truong Thi Ngoc Lien (IOP, HUST) for assistance in electrochemical measurements.

References

1 C. A. S. Hall, J. G. Lambert and S. B. Balogh, *Energy Policy*, 2014, **64**, 141–152.
2 A. Zabihallahpoor, M. Rahimnejad and F. Talebnia, *RSC Adv.*, 2015, **5**, 94171–94183.
3 A. S. Aricò, P. Bruce, B. Scrosati, J.-M. Tarascon and W. van Schalkwijk, *Nat. Mater.*, 2005, **4**, 366–377.
4 M. Shen, L. Ma, J. Zhu, X. Li and C. Wang, *RSC Adv.*, 2015, **5**, 59659–59664.
5 K. S. Kumar, N. Choudhary, Y. Jung and J. Thomas, *ACS Energy Lett.*, 2018, **3**, 482–495.

6 X. Lu, C. Wang, F. Favier and N. Pinna, *Adv. Energy Mater.*, 2017, **7**, 1601301.
7 C. Zhou, L. Lin, Y. Ma, L. Huang, J. Li, Z. Liu and Z. Dong, *ChemElectroChem*, 2017, **4**, 2314–2320.
8 H. Duan, T. Yan, Z. Li, G. Chen, J. Zhang, L. Shi and D. Zhang, *Sustainable Energy Fuels*, 2017, **1**, 1557–1567.
9 H. Duan, T. Yan, G. Chen, J. Zhang, L. Shi and D. Zhang, *Chem. Commun.*, 2017, **53**, 7465–7468.
10 F. Ghasemi, M. Jalali, A. Abdollahi, S. Mohammadi, Z. Sanaee and S. Mohajerzadeh, *RSC Adv.*, 2017, **7**, 52772–52781.
11 S. Hu, R. Rajamani and X. Yu, *Appl. Phys. Lett.*, 2012, **100**, 104103.
12 K. S. Ryu, K. M. Kim, N.-G. Park, Y. J. Park and S. H. Chang, *J. Power Sources*, 2002, **103**, 305–309.
13 G. Wang, L. Zhang and J. Zhang, *Chem. Soc. Rev.*, 2012, **41**, 797–828.
14 Z. Ren, J. Li, Y. Ren, S. Wang, Y. Qiu and J. Yu, *Sci. Rep.*, 2016, **6**, 20021.
15 Z. Yu, L. Tetard, L. Zhai and J. Thomas, *Energy Environ. Sci.*, 2015, **8**, 702–730.
16 F. Liu, X. Wang, J. Hao, S. Han, J. Lian and Q. Jiang, *Sci. Rep.*, 2017, **7**, 17709.
17 S. Ci, Z. Wen, Y. Qian, S. Mao, S. Cui and J. Chen, *Sci. Rep.*, 2015, **5**, 11919.
18 Y. Zheng, H. Ding and M. Zhang, *Mater. Res. Bull.*, 2009, **44**, 403–407.
19 Y. Chuminjak, S. Daothong, P. Reanpang, J. P. Mensing, D. Phokharatkul, J. Jakmunee, A. Wisitsoraat, A. Tuantranont and P. Singjai, *RSC Adv.*, 2015, **5**, 67795–67802.
20 J. Cheng, B. Zhao, W. Zhang, F. Shi, G. Zheng, D. Zhang and J. Yang, *Adv. Funct. Mater.*, 2015, **25**, 7381–7391.
21 N. Liu, J. Li, W. Ma, W. Liu, Y. Shi, J. Tao, X. Zhang, J. Su, L. Li and Y. Gao, *ACS Appl. Mater. Interfaces*, 2014, **6**, 13627–13634.
22 H. Xiao, S. Yao, H. Liu, F. Qu, X. Zhang and X. Wu, *Prog. Nat. Sci.: Mater. Int.*, 2016, **26**, 271–275.
23 Z. Lu, Z. Chang, J. Liu and X. Sun, *Nano Res.*, 2011, **4**, 658–665.
24 Q. Yang, J. Sha, X. Ma and D. Yang, *Mater. Lett.*, 2005, **59**, 1967–1970.
25 B. R. Cruz-Ortiz, M. A. Garcia-Lobato, E. R. Larios-Durán, E. M. Múzquiz-Ramos and J. C. Ballesteros-Pacheco, *J. Electroanal. Chem.*, 2016, **772**, 38–45.
26 M. Yu, J. Liu and S. Li, *J. Univ. Sci. Technol. Beijing*, 2006, **13**, 169–173.
27 F. L. Zhu and Y. S. Meng, *Adv. Mater. Res.*, 2013, **668**, 331–334.
28 H. Chai, X. Chen, D. Jia, S. Bao and W. Zhou, *Mater. Res. Bull.*, 2012, **47**, 3947–3951.
29 D. Su, H.-S. Kim, W.-S. Kim and G. Wang, *Chem.–Eur. J.*, 2012, **18**, 8224–8229.
30 Y. Jiang, Z. Jia, W. Zhang and H. Suo, *J. Inorg. Organomet. Polym. Mater.*, 2013, **23**, 1043–1047.
31 S. Cao, W. Zeng, T. Li, J. Gong and Z. Zhu, *Mater. Lett.*, 2015, **156**, 25–27.
32 S. Safa, R. Hejazi, M. Rabbani and R. Azimirad, *Desalin. Water Treat.*, 2016, **57**, 21982–21989.
33 G. Li, X. Wang, L. Liu, R. Liu, F. Shen, Z. Cui, W. Chen and T. Zhang, *Small*, 2015, **11**, 731–739.
34 T. T. Le Dang, M. Tonezzer and V. H. Nguyen, *J. Nanomater.*, 2015, **2015**, 1–8.
35 N. D. Hoa and S. A. El-Safty, *Chem.–Eur. J.*, 2011, **17**, 12896–12901.
36 P. Van Tong, N. D. Hoa, N. Van Duy, V. Van Quang, N. T. Lam and N. Van Hieu, *Int. J. Hydrogen Energy*, 2013, **38**, 12090–12100.
37 D. Su, M. Ford and G. Wang, *Sci. Rep.*, 2012, **2**, 924.
38 C. W. Kim, Y. S. Son, A. U. Pawar, M. J. Kang, J. Y. Zheng, V. Sharma, P. Mohanty and Y. S. Kang, *J. Mater. Chem. A*, 2014, **2**, 19867–19872.
39 M. A. Peck and M. A. Langell, *Chem. Mater.*, 2012, **24**, 4483–4490.
40 R. Fahim, *J. Catal.*, 1970, **17**, 10–17.
41 X. Qing, S. Liu, K. Huang, K. Lv, Y. Yang, Z. Lu, D. Fang and X. Liang, *Electrochim. Acta*, 2011, **56**, 4985–4991.
42 S. Ibrahim, T. Charinpanitkul, E. Kobatake and M. Sriyudthsak, *J. Chem.*, 2016, **2016**, 1–6.
43 B. Vidhyadharan, N. K. M. Zain, I. I. Misnon, R. A. Aziz, J. Ismail, M. M. Yusoff and R. Jose, *J. Alloys Compd.*, 2014, **610**, 143–150.
44 J. W. Lee, T. Ahn, J. H. Kim, J. M. Ko and J.-D. Kim, *Electrochim. Acta*, 2011, **56**, 4849–4857.
45 N. Elgrishi, K. J. Rountree, B. D. McCarthy, E. S. Rountree, T. T. Eisenhart and J. L. Dempsey, *J. Chem. Educ.*, 2018, **95**, 197–206.
46 Y. Wan, Y. F. Zheng, B. Zhou and X. C. Song, *J. Nanosci. Nanotechnol.*, 2018, **18**, 3585–3591.
47 A. Allagui, A. H. Alami, E. A. Baranova and R. Wüthrich, *J. Power Sources*, 2014, **262**, 178–182.